Heliyon 7 (2021) e07061

Contents lists available at ScienceDirect

Heliyon

journal homepage: www.cell.com/heliyon

Research article

Speculative assessment, molecular composition, PDOS, topology exploration (ELF, LOL, RDG), ligand-protein interactions, on 5-bromo-3-nitropyridine-2-carbonitrile

K. Arulaabaranam [a,b], S. Muthu [a,c,*], G. Mani [a], A.S. Ben Geoffrey [d,e]

[a] Department of Physics, Arignar Anna Govt. Arts College, Cheyyar, 604407, Tamilnadu, India
[b] Thiruvalluvar University, Serkadu, Tamilnadu, India
[c] Department of Physics, Puratchi Thalaivar Dr.M.G.R. Govt. Arts and Science College, Uthiramerur, 603406, India
[d] Department of Physics, Madras Christian College, East Tambaram, 600059, Tamilnadu, India
[e] University of Madras, Chepauk, Chennai, 005, Tamilnadu, India

ARTICLE INFO

Keywords:
PES
ELF
RDG
PDOS
Molecular docking
MD simulations

ABSTRACT

Computational calculations of 5-bromo-3-nitropyridine-2-carbonitrile (5B3N2C) on molecular structure and on energy are implemented using the 6-311++G(d,p) basis set by DFT/B3LYP method. The UV-Vis spectrum of 5B3N2C was obtained by TD-DFT with chloroform as a solvent. The analysis of molecular electrostatic potential (MEP) and frontier molecular orbital (FMO) were used to evaluate, the entire electron density and organic reactive sites of 5B3N2C. The electron-hole conversions were conjointly deliberated. Donor-acceptor interactions (NBO) analysis examines the intra-and intermolecular charge transfer, hyper conjugate interaction of the compound. The orbital molecular contributions are evaluated by density of states (DOS and PDOS). To discern the reactivity of the molecule, topology analyses were done. The biological prominence of the 5B3N2C molecule was investigated in a pertinent study of molecular docking with target protein 3CEJ exhibiting the centromere associated protein inhibitor property. Molecular Dynamics simulations were done to assess the stability of the complex. 5B3N2C physiochemical parameters were also compared to those of widely viable medications Ispinesib and Lonafarnib.

1. Introduction

The resonance occurs in pyridine, pyrazine, and similar six-membered heterocyclic compounds, allowing the molecule to be planar and stable, much as it does in benzene. Pyridine is peculiar in that it is the azine that is also closest to benzene [1, 2, 3]. The widespread applicability of the halogen in material science, medical chemistry, molecular recognition processes, catalysis, crystal engineering of halogen bearing compounds and drug design (30–40%) is notable [4]. The widely dispersed pyridine ring systems in nature include niacin, vitamin B6, nicotinamide and strychnine. Vitamin B5, vitamin B6,pyridoxal, and pyridoxamine, as well as medications like Nifedipine, Nichetamine, and Sulphapyridine, all contain the pyridine ring [5, 6, 7, 8]. Organic light-emitting diodes (OLEDs) based on thermally activated delayed fluorescence (TADF) have been beheld as the modern millennium of the OLEDs. With a view to diminish the power ingesting of full-colour OLEDs, high-performance blue emissions are very decisive [9]. To date, a donor-acceptor (D-A)-or D-A-D-type architecture, is typically used to build TADF emitters. By means of restricted acceptors, such as xanthone, sulfone, benzoylpyridine, phosphine oxide, pyrimidine, *pyridine-carbonitrile*, oxa-diazole, triazine, phthalonitrile, and their derivatives, a small number of exceedingly proficient blue TADF emitters have been testified based on this stratagem. Multiple groups have documented pyridine-carbonitrile based TADF constituents in which pyridine-carbonitrile is designed as the acceptor [10, 11].

The designated molecule is 5-Bromo-3-nitropyridine-2-carbonitrile (5B3N2C) with molecular formula $C_6H_2BrN_3O_2$ and molecular weight 228.00 g/mol. This compound is easy to synthesis and is readily available from Sigma at 98% purity. Chromenopyridines are heterocyclic molecules fused with a broad variety of biological activities: a) antibacterial b) antiproliferative (cytotoxic action against the HT-29 cell lines of the human solid tumour) c) cancer chemopreventive d) antirheumatic e)

* Corresponding author.
E-mail address: mutgee@gmail.com (S. Muthu).

https://doi.org/10.1016/j.heliyon.2021.e07061
Received 5 January 2021; Received in revised form 18 March 2021; Accepted 11 May 2021

antihistaminic f) antimyopic and e) antiasthmatic [12, 13]. For the synthesis of insecticides, herbicides, medicinal products, supplements, food flavourings, food additives, synthetic compounds, detonators, antimicrobials, and sealants, the pyridine and its components are reused as solvents and as the starting material [14, 15, 16]. Real and synthetic compounds with the cyanopyridine moiety have also validated imperative antibacterial and antifungal activities in assessment to biologically active compounds with a carbon-nitrogen bond [17, 18, 19, 20]. The review of literature connotes that the no DFT studies have been done on the 5-Bromo-3-nitropyridine-2-carbonitrile thus far. Despite the fact, that the molecule that investigated in the present study retains several biological properties, the centromere associated protein inhibitor property was preferred to attest the biological competence of 5B3N2C molecule by molecular docking. It is a mitotic kinesin associated with kinetochore that is believed to serve as the crucial receptor responsible for transduction of mitotic checkpoint signal after interface with spindle microtubules (tumour cell apoptosis and tumour regression). Herein existing effort with the optimized molecular structure, electronic properties, hole-electron distribution, the energy gap, non-linear optical (NLO), natural bond orbital (NBO), topology analysis, thermodynamic properties, ADMET and molecular docking of the designated molecule are conferred.

2. Computational details

The 5B3N2C molecule was optimized by DFT method with B3LYP/6-311++G(d,p) basis set [21, 22, 23]. The theoretical UV-Vis spectrum was simulated by the TD-DFT/B3LYP method using IEFPCM Model and chloroform as a solvent [24]. GaussSum were used to plot the graphs for UV-Vis, DOS and PDOS [25]. The MEP surface and the FMO were mapped by the GaussView 5.0 [26]. The ELF and LOL were plotted with Multiwfn 3.4.1, a wave function software analyser [27]. AutoDock Suite 4.2.1 finds out the minimum binding energy, inhibition constant and various parameters of the ligand-protein interactions [28, 29]. To visualize the parameters of the ligand –protein interactions Discovery Studio 4.1 Visualizer software was used [30]. Protein-Protein interaction, DNA-DNA interaction, DNA-Protein interaction, and Protein-ligand interaction can all be examined utilizing software packages that use different forms of these force fields. The CHARMM force field was used in conjunction with the GROMACS kit to investigate the protein-ligand interaction involving the centromere associated protein inhibitory and ligand 5B3N2C in this analysis. The GROMACS software package was used to execute the molecular dynamics simulations [31].

3. Result and discussion

3.1. Potential energy scan and molecular geometry

The potential energy (PES) scan analysis is performed for dihedral angles O_2-N_5-C_7-C_8 using B3LYP/6-311++G(d,p) method for the 5B3N2C molecule is symbolised in Figure 1 and are charted in Table 1. During the calculation all the geometrical parameters were varied in steps of 10°. For this rotation, the conformational energy profile shows four minima at step number 3, 17, 21 and 35 are same with the energy values -3118.6977 Hartree (-1957012.7901 kcal/mol). It is clear that there is two maxima at step number 10, 28 are same with the energy values -3118.6940 Hartree (-1957010.4808 kcal/mol). The two minima (3 and 17) and the other two minima (21, and 35) befalling at disparity of step number are not similar for the reason that the nitrile group are acting oppositely but dynamically both are equal with values of -3118.6977 Hartree (-1957012.7901 kcal/mol).

The 5B3N2C molecule has been enumerated with optimized structural parameters in Table 2, which compared with the XRD value of structurally related pyridine 3-carbonitrile derivatives [32]. To the best of our knowledge, the literature does not include reliable laboratory evidence on the geometrical parameters of

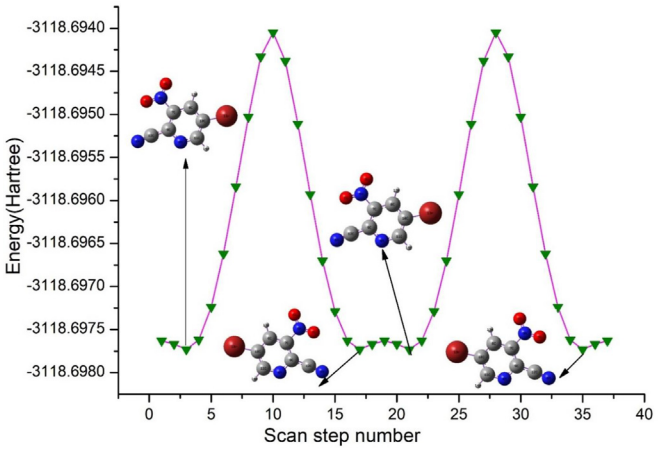

Figure 1. Potential energy scan (PES) is performed for dihedral angles O2-N5-C7-C8 using B3LYP/6-311++G(d,p) method for the 5B3N2C molecule.

Table 1. Potential energy surface scan analysis for 5B3N2C molecule with step number for the dihedral angle O_2-N_5-C_7-C_8 using B3LYP/6-311++G(d,p) method.

Scan step number	Scan co-ordinate()	Total energy(Hartree)
1	-180	-3118.69763
2	-170	-3118.69767
3	-160	-3118.69773
4	-150	-3118.69762
5	-140	-3118.69724
6	-130	-3118.69662
7	-120	-3118.69584
8	-110	-3118.69503
9	-100	-3118.69433
10	-90	-3118.69405
11	-80	-3118.69438
12	-70	-3118.69511
13	-60	-3118.69593
14	-50	-3118.69670
15	-40	-3118.69729
16	-30	-3118.69763
17	-20	-3118.69773
18	-10	-3118.69767
19	0	-3118.69763
20	10	-3118.69767
21	20	-3118.69773
22	30	-3118.69763
23	40	-3118.69729
24	50	-3118.69670
25	60	-3118.69593
26	70	-3118.69511
27	80	-3118.69438
28	90	-3118.69405
29	100	-3118.69433
30	110	-3118.69503
31	120	-3118.69584
32	130	-3118.69662
33	140	-3118.69724
34	150	-3118.69762
35	160	-3118.69773
36	170	-3118.69767
37	180	-3118.69763

Table 2. The optimized structural parameters of the 5B3N2C molecule calculated by the B3LYP/6-311++G(d,p) basis set.

Parameters	Bond length (A)	
	DFT/6-311++G(d,p)	Expt*
Br1-C10	1.898	1.890
O2-N5	1.223	-
O3-N5	1.218	-
N4-C9	1.342	1.341
N4-C11	1.327	1.340
N5-C7	1.486	1.441
N6-C12	1.154	1.140
C7-C8	1.389	1.384
C7-C9	1.404	1.406
C8-C10	1.386	1.379
C8-H13	1.081	0.970
C9-C12	1.438	1.426
C10-C11	1.398	1.395
C11-H14	1.085	0.970
	Bond Angle ()	
Br1-C10-C8	120.8	119.5
Br1-C10-C11	120.2	119.3
O2-N5-O3	125.7	-
O2-N5-C7	117	-
O3-N5-C7	117.4	-
C9-N4-C11	119.6	-
N4-C9-C7	120.7	120.6
N4-C9-C12	114.4	114.6
N4-C11-C10	122.6	124.6
N4-C11-H14	116.7	117.7
N5-C7-C8	117.4	118.9
N5-C7-C9	122.5	124.4
N6-C12-C9	174.2	178.5
C8-C7-C9	120.1	119.7
C7-C8-C10	117.9	117
C7-C8-H13	119.5	119.7
C7-C9-H12	125	120.7
C10-C8-H13	122.5	120.2
C8-C10-C11	119	119.5
C10-C11-H14	120.7	120.7

* - As per reference [31].

5-bromo-3-nitropyridine-2-carbonitrile. The geometry optimization was accomplished to find the utmost established arrangement of molecule. The molecule has 2 merged non-polar hydrogens, 5 aromatic carbons and 1 rotated bond. With 6-311++G(d,p) basis set, the 5B3N2C molecule is optimized by means of the DFT/B3LYP progression. The optimised structure of the labelled molecule with atom numbering and bond length is specified in Figure 2. The designated molecule's molecular geometry has C1 point group symmetry. The molecule has four N-C bonds, five C-C bonds, two C-H, O-N bonds, and one Br-C bond. The optimised pyridine ring N4-C9 and N4-C11 bond lengths are in the range DFT/XRD; 1.342/1.341 and 1.327/1.340Å. The N6-C12 bond of the nitrile group have slighter lower bond length (1.154/1.140Å) compared to the other N-C bond because of the triple bond. The O2-N5 and O3-N5 bond of the nitro group has bond length 1.223 and 1.218Å. The homoatomic bond C9-C12, C7-C8, C7-C9, C8-C10, C10-C11, has the bond length in the range 1.438–1.389/1.426-1.384Å. The heteroatomic bond have lower bond length compared to homoatomic bond. The C8-H13, C11-H14 have lower bond lengths 1.081/0.970, 1.085/0.970Å. The Br1-C10 bond has the largest bond length 1.898/1.890Å out of all the bond lengths.

3.2. Non-linear optical analysis

Owing to the movement of protons from the electron donor group to the electron acceptor group induces a higher molecular first order hyper polarizability which contributes to a higher susceptibility in an organic molecule [33]. In general, because of the lone pair of electrons, heterocyclic nitrogen containing aromatic compounds such as pyridine and its components give favourable conditions for NLO [34, 35]. This research premeditated the electronic dipole moment, molecular polarizability, polarizability of anisotropy, and the first molecular hyper polarizability of the current compound. The polarizability (α), the hyper polarizability (β), and the electric dipole moment (μ) of the 5B3N2C compound are determined using the B3LYP/6-311++G(d,p) basis available in the Gaussian 09 package. A Gaussian frequency job output file can be used to obtain polarizability and hyper polarizability tensors (α_{xx}, α_{xy}, α_{yy}, α_{xz}, α_{yz}, α_{zz} and β_{xxx}, β_{xxy}, β_{yyy}, β_{xyz}, β_{yyz}, β_{xzz}, β_{yzz}, β_{zzz}). The molecular hyper polarizability β of the designated molecule has been calculated as 4.5553 $\times 10^{-30}$ esu with dipole moment 2.5550 Debye and 5.3795 $\times 10^{-23}$ e.s.u using Gaussian output by DFT/B3LYP/6-311++G(d,p) set and the values have been made known in Table 3. 4.5553 $\times 10^{-30}$ e.s.u is the measured first order hyper polarizability of the studied compound, which is five times greater than the standard NLO substance Urea ($\beta = 0.967 \times 10^{-30}$). It could be inferred, on the basis of these evidence, that the material present has a fairly good tendency for non-linear optical operation.

3.3. Electronic properties and frontier molecular orbitals

The theoretical absorption spectra of the optimized 5B3N2C compound are calculated in the solvent chloroform using the TD-B3LYP/6-311++G(d,p) level of theory with IEFPCM model [36]. The orbitals of molecule involved in the absorption spectrum of the compound are displayed in Figure 3. The absorption wavelength obtained using TD-DFT method is reported in Table 4. The maximum wavelength with the highest oscillation of the 5B3N2C molecule is observed at 289nm and its oscillator strength f = 0.0946. The theoretical calculation shows transition (HOMO)→(LUMO) was the most important charge transmission

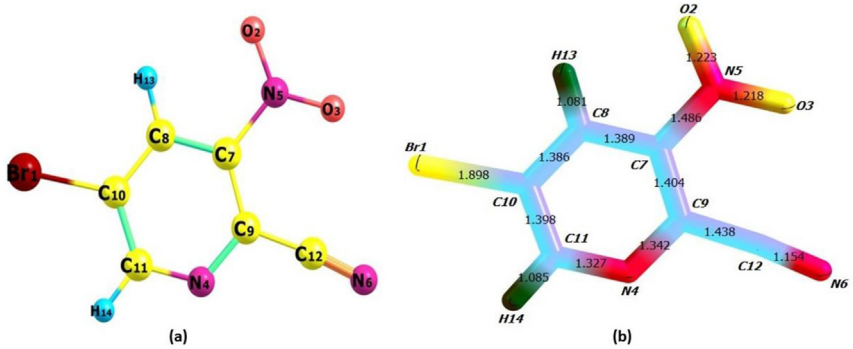

Figure 2. The optimised structure of 5B3N2C molecule with (a) atom numbering and (b) bond length using B3LYP/6-311++G(d,p) basis set.

Table 3. Calculated first order hyperpolarizability (β), polarizability(α), dipole moment) components of the 5B3N2C molecule.

Parameters	B3LYP/6-311++G(d,p)
βxxx	-351.255
βyyy	-13.4313
βzzz	-145.793
βxyy	-153.68
βxxy	-0.15176
βxxz	0.1111
βxzz	-0.00543
βyzz	52.88031
βyyz	-0.29792
βxyz	0.02486
βtot (a.u)	527.0862
βtot (e.s.u)	4.55E-30
αxx	183.6401
αyy	-13.7693
αzz	121.89
αxy	-0.00421
αxz	-0.00029
αyz	58.8665
α (α.u)	97.25359
α (e.s.u)	1.44E-23
Δα (α.u)	362.9939
Δα (e.s.u)	5.38E-23
μx	2.55465
μy	-0.04318
μz	0.00038
μ(D)	2.555015

within the compound that belong to the transition of one electron into the excited state S0→S2 with 93%. The excitation of one electron at 310nm (f = 0.009) belong to the transition into the state S0→S1, describes by a wave function corresponding to a superposition of three configurations [(HOMO-8→LUMO), (HOMO-7→LUMO), (HOMO-4→LUMO)] with the bandgap values of 3.2422, 4.0058, 4.2968eV.

In Figure 4, the population analysis of Mulliken was computed and plotted. They give a graphical depiction of orbital molecular compositions and their chemical bonding contributions from Figure 4. The structure of fragment orbitals belonging to molecular orbitals is

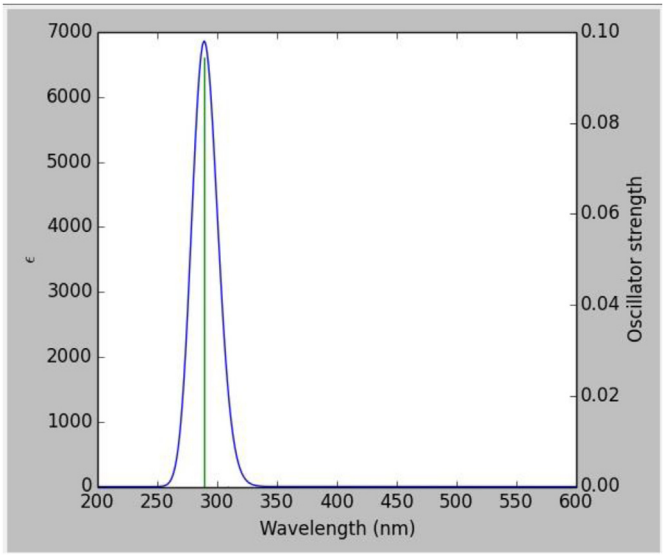

Figure 3. Simulated UV-Vis absorption spectra of 5B3N2C molecule with chloroform as solvent with TD-DFT/6-311++G(d,p).

Table 4. The UV-Vis wavelength (λ), band gap energy(eV) and oscillator strength (f) for title compound computed by TD-DFT/6-311++G(d,p).

Energy (cm-1)	Wavelength (nm)	Osc. Strength (f)	Energy gap (eV)	Major contributions
26109	383	0	3.2422	H-7- > LUMO (11%), H-2- > LUMO (70%)
32309	310	0.0002	4.0058	H-8- > LUMO (16%), H-7- > LUMO (44%), H-4- > LUMO (19%)
34579	289	0.0946	4.2968	HOMO- > LUMO (93%)

λ- Wavelength, nm-nanometre, f-oscillator strength eV-electron volt, HOMO-Highest occupied molecular orbital, LUMO - Lowest unoccupied molecular orbital.

exemplified in DOS and PDOS plots. The colour green represents HOMO and the colour red represents the orbital LUMO. The positive value of the PDOS was validated by a bonding interaction, while an anti-bonding interaction advocates that negative values and non-binding interactions represent values close to zero. Quasi-degenerate energy levels of neighbouring orbitals may arise in the boundary region. On the nitro group, bromine atom and pyridine ring, the HOMO orbital is confined. On the nitro group and bromine atom, the LUMO orbital is confined.

The FMO studies includes data on molecule's reactivity and stability [37]. The plot of HOMO and LUMO reveals the passage of charges within the molecule. Figure 5 displays the HOMO and LUMO plots. HOMO and LUMO are found to be localized in the molecule as yellow (negative position) and blue (positive position) colour. HOMO is localized in the 5B3N2C molecule over the pyridine ring (except N_4 atom), nitrile group ($C_{12}\equiv N_6$), and bromine atom. LUMO is positioned over the nitro group, pyridine ring (except N_4 atom), N_6 atom. If the value of the E_{HOMO} is high, it designates the ease of bestowing electron to the vacant orbital of the receptor molecule. If the value of E_{LUMO} is lesser, it means it has a lesser resistance to admit electrons so it will be further capable to admit electron. The HOMO and LUMO energy values of the 5B3N2C molecule are exhibited in Table 5 and are interrelated to the ionization potential (I) = - E_{HOMO} = 8.3229eV and electron affinity (A) = - E_{LUMO} = 3.9326eV. The energy gap is attained from the difference between the HOMO and LUMO energy values (Eg) = 4.3903eV. The low energy values of I, A, and Eg defines that the 5B3N2C molecule has lower solidity and utmost reactivity. The chemical potential (μ) = -6.1278eV stretches a hint about the charge transmission within the 5B3N2C molecule in its ground state. The electrophilic index (ω) = 8.5528eV describes the chemical reaction of the molecule i.e. sturdily electrophilic in nature. The electronegativity (χ) = 6.1278 eV, outlines the ability of the molecule to attract electrons towards itself in a covalent bond i.e. 5B3N2C is the utmost electron acceptor. The chemical hardness (η) = 2.1952, outlines that the 5B3N2C molecule is chemically firmest.

3.4. Electron-hole analysis

The excitation properties of electrons can be thoroughly explored by the study of electrons and holes. Since the UV spectrum consists mainly of the conversion from the ground state to excited states, the study of the electron-hole is carried out only on the three excited states [38]. The distribution of the electron-hole is showcased in Figure 6, where electrons are portrayed by green and holes are portrayed by blue. The appropriate electron-holes distribution strictures are portrayed in Table 6. The distance between the electron and the hole centroid is expressed by the factor D. The Δr is a feature which depicts the overlap between distributions of electron-holes. The values vary between 0 to 1. The substantial the value of Δr, the greater the degree of overlap between holes and electrons. The substantial lower the value of Δr, the lower the degree of overlap between holes and electrons. Figure 6 displays the Δr diagram of these three excited states. Bestowing to the hole –electron distribution maps for the third excited state the hole and electrons are

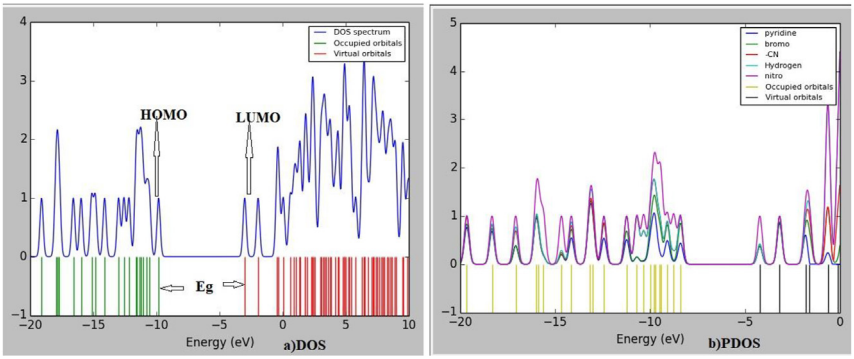

Figure 4. Plot of (a)DOS and (b)PDOS spectra of 5B3N2C molecule.

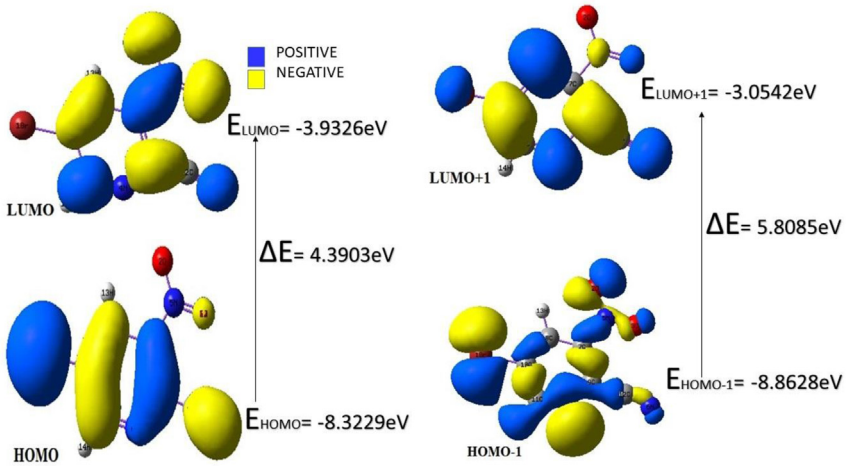

Figure 5. The atomic orbital compositions of the frontier molecular orbital for 5B3N2C molecule.

almost dispersed entirely on the pyridine ring and the bromine atom. It can be revealed from the table that the charge transfer length of the transition mode 3 (1.756Å) compared with the other 1 and 2 states (1.131 Å and 1.271 Å respectively), the third excitation mode is significantly larger and Δr is conjointly higher for the same mode. Thus suggesting that a heavy charge transfer excitation corresponds to the third excitation mode.

3.5. Topology analyses

3.5.1. ELF and LOL analysis

The techniques used to estimate the concentration of electron density in the compounds are electron localization function (ELF) and localized orbital locator (LOL) [39]. They both perform the covalent bond analysis, and disclose the regions of molecular space where the prospect of verdict on an electron pair is high [40, 41]. The colour filled projection map and vector field of ELF and LOL with contour map obtained from Multiwfn program of the 5B3N2C molecule are displayed in Figures 7 and 8. These maps are designed in the range of 0–1.0, denoting that they have analogous chemical contents. If the plotted value of ELF is in the region 0.5–1.0, then they have bonding and nonbonding localized electrons, whereas value is in the region <0.5, then they have delocalized electrons. Though the interpretation are analogous, LOL expresses a further conclusive and flawless depiction than ELF. The red colour represents the higher end of the scale, and the blue colour represents the lower end of the scale. The regions around C11, C10, C12, N4, N6, N5 where the electrons are projected to be delocalized because of its lesser values, whereas the regions around H14 suggest that the bonding and non-bonding electrons are highly localized. In LOL, the red regions that are presented between carbon atoms and carbon-nitrogen atoms, C10-C11, C11-N4, C12-N6, are the covalent regions with high LOL value.

Table 5. Calculated quantum chemical parameters of 5B3N2C molecule.

Chemical Parameters	B3LYP/6-311++G(d,p)
HOMO(eV)	-8.3229
LUMO(eV)	-3.9326
Ionization potential	8.3229
Electron affinity	3.9326
Energy gap(eV)	4.3903
Electronegativity	6.1278
Chemical potential	-6.1278
Chemical hardness	2.1952
Chemical softness	0.2278
Electrophilicity index	8.5528

3.5.2. Reduced density gradient

As a mechanism for disclosing non-covalent interactions, a reduced density gradient feature has been implemented. Interactions move from weak to strong alongside reactions and vice versa, and RDG forms the base of reactivity studies [42]. In order to forecast the real space weak interaction based on electron density, RDG analysis is used and it is a dimension less quantity and it is first derived by Eq. I(I)

$$\mathrm{RDG} = \left(\mathrm{r}\right) = \frac{1}{2(3\pi r^2)^{1/3}} \frac{|\Delta^2\ (\rho(\mathrm{r})|}{(\rho(\mathrm{r})^{4/3})} \qquad \text{(I)}$$

Low electron region can be defined by assessing the low density gradient, which is concerned with weak interaction, whereas the high

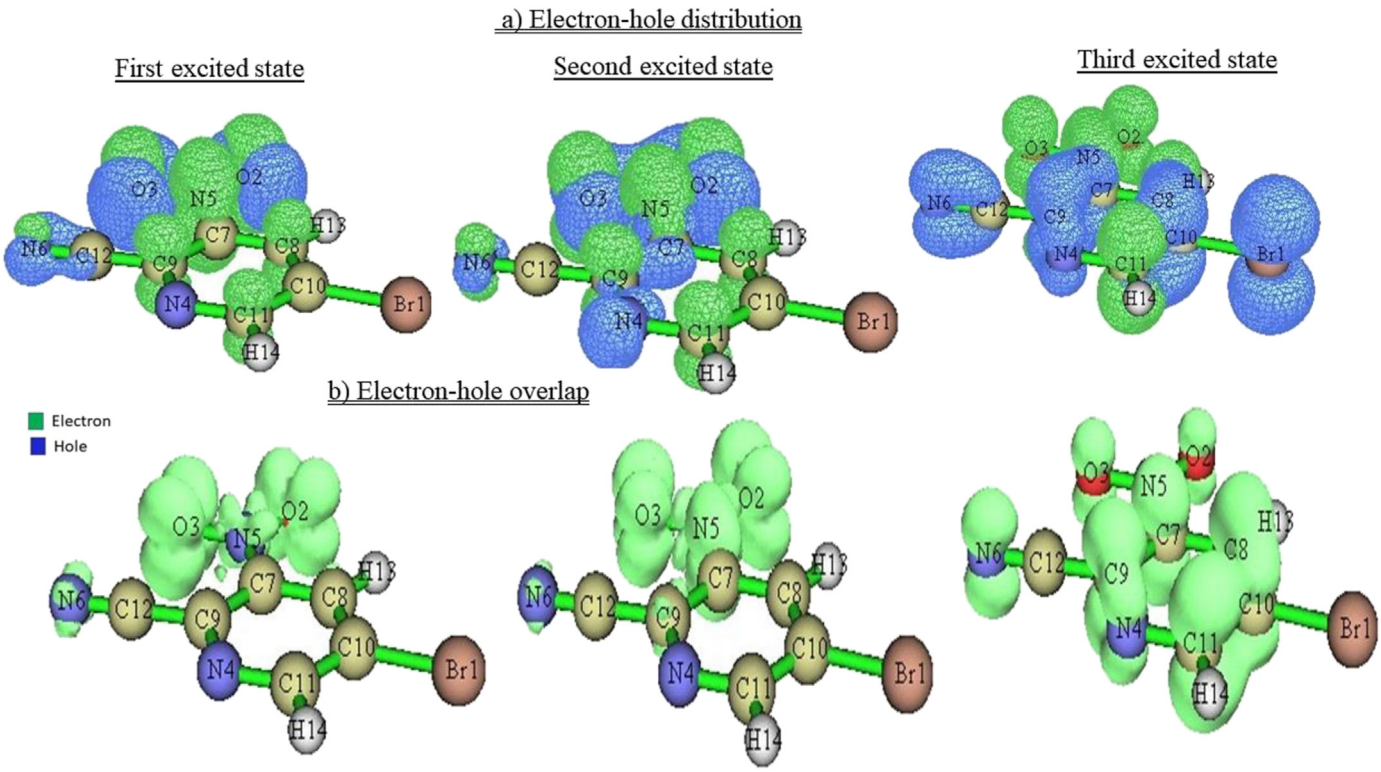

Figure 6. (a) Electron-hole distribution, (b) overlap-integral of the three excited states of 5B3N2C molecule.

Table 6. The charge transfer length (Å), Δr index, excitation energy (eV) of the 5B3N2C molecule in different excitation state.

Excitation state	Excitation energy(eV)	Integrals of transition density	Δr index	Charge-transfer length(Å)
State1	3.208	0.000056	1.3368	1.131
State2	4.001	0.000008	1.5613	1.371
State3	4.33	-0.000163	2.2651	1.756

density gradient value was used to localize the strong interaction [43]. RDG was designed using the Multiwfn programme, scatter graph and colour/contour filled RDG for the compound is seen in Figure 9. The 2D scatter plots for the 5B3N2C compound of RDG versus sign (λ^2) ρ(r) included on Figure 9 of the noncovalent associations in the labelled molecule have simple fingerprints. A greater enticing ($\lambda^2 < 0$) or repulsive ($\lambda^2 > 0$) non-covalent interaction is demonstrated by a higher absolute value of electron density at the interaction of critical points. The relationship of intensity in the molecular structure, in which blue colour signifies greater attraction, the red colour reflects the ring system which is responsible for the steric effect. This compound emits the green colour that reflects the contact between van der Walls, i.e. non-covalent interaction that might have been liable for the labelled compound's stabilization.

3.6. Molecular electrostatic potential, electrostatic potential, and total electron density

The MEP, ESP, and TED surfaces of 5B3N2C molecule are computed by theoretical calculations using the B3LYP/6-311++G(d,p) basis set. A uniform distribution displays the TED plots for the 5B3N2C molecule. Although it can be seen from the ESP statistic that the negative ESP is more concentrated and expressed as a greenish colour over the molecule's oxygen O2, O3 atoms and nitrogen N6 atom (Figure 10). This is expected since ESP correlates with electronegativity and partial charges. The MEP

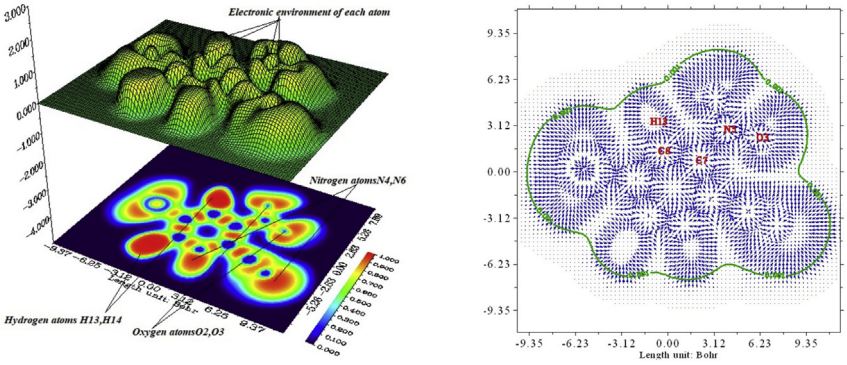

Figure 7. The (a) relief map with projection and (b) vector map of ELF of 5B3N2C molecule.

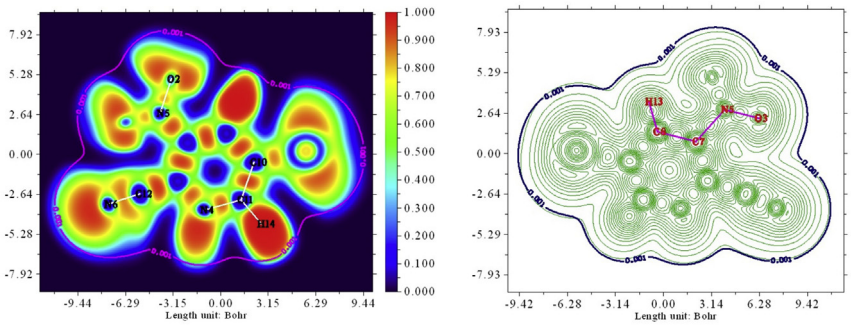

(a) (b)

Figure 8. Colour filled (a) and contour LOL(b) map of 5B3N2C molecule.

map detects the negative and positive electrostatic potentials regions for electrophilic attacks and nucleophilic reactions by the electron density of the molecule [44, 45]. The MEP is mapped in the spectrum of -4.715e-2 (deepest red) portraying the electron attraction caused by excessive electron density and +4.715e-2 (deepest blue) portraying the proton repulsion by atomic nuclei attributable to shades of low electron density. The MEP surface with contour map is depicted in the Figure 10. From the Figure 10, the contour plots the electron rich red lines around hetero-atoms, whilst the unpaired electron region is shown by greenish-yellow lines. The negative electrostatic potential sites (red and yellow) of the 5B3N2C molecule is located around the O2, O3, N_5 of nitro group, N_6 of nitrile group, and N_4 of the pyridine ring because of the intermolecular bonding interactions. The positive potential site (blue) is located around the carbon, and hydrogen atoms H_{13}, H_{14} of the pyridine ring. The regions in green colour around the bromine Br1 atom indicates zero potential. These regions of reactivity are responsible for demonstrating the bioactivity of the molecule.

3.7. Donor-acceptor interactions

In the equilibrium of the molecule, intramolecular interaction and the formation of hydrogen bonds play a prominent part and make the molecule relatively stable. The study of intra- and inter-molecular bonding and contact between bonds in molecular systems are scrutinised by natural bond orbital analysis [46]. NBO analysis of the 5B3N2C compound with B3LYP/6-311++G(d,p) level of energy was conducted with the aim of clarifying the intra-molecular, rehybridization and delocalization of electron density within the compound,. The stabilizing connection is expressed in terms of second-order interaction energy of micro disturbance E(2) are conveyed in Table 7. Because of the lone pairs of oxygen atom LP(3)O2 →O3-N5 with the stabilisation energy of 155.05 kcal/mol, the NBO analysis predicted a strong n→π* interactions. The sturdy stabilisation interaction between LP(2) O2→σ*(O3-N5) and LP(2)O2→σ*(O2-N5) with the stabilisation energy of 17.37 and 18.03 kcal/mol was also achieved. Compared with σ→σ* transitions, the intermolecular hyper conjugative interactions of the π→π* transitions have the most resonance energy ED/e. For instance N4-C9→C7-C8, C10-C11 with the strong resonance energies 217.15 and 200.38 kcal/mol are the noteworthy intramolecular hyper conjugative interaction of the π*→π* transitions in pyridine ring that lead to a robust delocalization. The π→π* transitions have the highest energies compared with other interactions of the 5B3N2C compound. The characteristic feature of the pharmaceutical molecule is these interactions between the LP→σ*or π* orbitals.

Table 7. The Second order pertubation theory analysis of 5B3N2C molecule by NBO method using B3LYP/6-311++G(d,p).

Lewis base(α)		ED/e	Lewis acid(β)		ED/e	E(2)[a] kcal/mol	E(j)-E(i)[b] a.u	F(i,j)[c]a.u
σ	N 6 - C12	1.99459	σ*	C 9 - C12	0.03925	6.72	1.51	0.091
σ	C 7 - C 8	1.96535	σ*	Br 1 - C10	0.03162	4.78	0.84	0.057
σ	C 7 - C 9	1.97102	σ*	N 6 - C12	0.01047	4.47	1.68	0.078
π	O3 - N5	1.97833	π*	O 3 - N5	1.4453	7.56	0.3	0.051
π	N4 - C9	1.68843	π*	C7 - C8	0.34794	13.84	0.31	0.059
π	C7 - C8	1.61294	π*	O3 - N5	0.63533	32.86	0.15	0.068
π	C7 - C8	1.61294	π*	N4 - C9	0.42092	31.25	0.27	0.083
π	C7 - C8	1.61294	π*	C10 - C11	0.33698	14.74	0.29	0.059
π	C10 - C11	1.60253	π*	N4 - C9	0.42092	14.52	0.27	0.056
π	C10 - C11	1.60253	π*	C7 - C8	0.34794	25.97	0.29	0.078
LP (2)	O2	1.90579	σ*	O3 - N5	0.0553	17.37	0.67	0.097
LP (3)	O2	1.4453	π*	O3 - N5	0.63533	155.05	0.13	0.129
LP (2)	O3	1.89477	σ*	O2 - N5	0.05672	18.03	0.67	0.099
LP (1)	N6	1.97156	σ*	C9 - C12	0.03925	11.99	0.99	0.097
LP (3)	Br1	1.91581	π*	C10 - C11	0.33698	11.52	0.29	0.055
π*	N 4 - C9	1.68843	π*	C 7 - C8	0.34794	217.15	0.02	0.085
π*	N4 - C9	1.68843	π*	C10 - C11	0.33698	200.38	0.02	0.081

[a] E (2) energy of hyper-conjugative interaction.
[b] Energy difference between donor and acceptor i and j NBO orbitals.
[c] F (i, j) Fock matrix element between i and j NBO orbitals.

3.8. ADMET and drug like nature assessment

Swiss ADME model were used to estimate and precise ADMET parameters like absorption, distribution, metabolism, excretion and toxicity [47]. The noteworthy biological activity of this compound may be arising from oxygen atoms of nitro group attached to the pyridine ring and the nitrogen to the nitrile group that can play a major role in centromere associated protein inhibitor (CENP-E). The drug like nature [48] descriptor of 5B3N2C molecule revealed from *molinspiration* program [49] in Table 8(a) reveals that the molecule possess 0 ($\leq$5) hydrogen bond donors and 5 ($\leq$10) hydrogen bond acceptors; the molecular weight of 5B3N2C found to be 228.00 (<500 g/mol). The topological surface area (TPSA) of this molecule possess 82.51 ($\leq$120$\mathring{A}^2$) and nrotb value is 1. The number of violations of this law revealed that there was a violation of 5B3N2C compound equal to zero, meaning that they would bind to the receptors quickly. The bioactivity score is 0.55, from the above values, it is established that the bioavailability of the designated molecule is active. The ADME prediction profiles are obtainable in Table 8(b). The blood brain barrier (BBB) penetration predicts that there is no penetration to cross the blood brain barrier, which indicates that it does not affect the central nervous system (CNS). The gastro intestinal (GI) absorption is high. The Log Kp skin permeation is -6.68; this value specifies that molecule cannot be absorbed by human skin. The pure water solubility were found to be low value; the values are -2.439. This 5B3N2C evidently less toxic as a result of this. Since the 5B3N2C molecule is a non-inhibitor of P-glycoprotein, consequently it does not interfere with the P-glycoprotein's in drug absorption and excretion. It is an inhibitor of CYP1A2 enzyme and non-inhibitor of CYP2C19, CYP2C9, CYP2D6, CYP3A4 enzymes. This concern stipulates that this molecule can be preserved as an imminent aspirant for bioactive claims.

The studied molecule and proven consumer cancer drugs Ispinesib, and Lonafarnib, the values are compared in Table 8(a). Lonafarnib, like CENP-E inhibitors, can suppress protein prenylation and cause cellular effects and phenotypes. In terms of clinical trials, lonafarnib has reached phase III and is considered one of the most successful. The cancer drugs Ispinesib and Lonafarnib has two violations in drug likeness, whereas the

Table 8(a). Molinspiration property values of 5B3N2C and standard drug molecule.

Descriptors	5B3N2C	Ispinesib	Lonafarnib	Expected range
Hydrogen bond donor (HBD)	0	1	1	<5
Hydrogen bond acceptors (HBA)	4	4	3	<10
AlogP	1.77	4.6	5.84	<5
Polar surface area (PSA) Å 2	82.5	81.23	79.53	<140
Molecular weight (dalton)	278	517.07	638.82	<500
Number of rotatable bonds	1	9	5	<10
Molar refractivity	45.47	150.85	157.3	40–130

Table 8(b). ADME properties of 5B3N2C molecule.

Property	Model Name	Predicted Value	Unit
Absorption	Water solubility	-2.439	Numeric (log mol/L)
Absorption	Caco2 permeability	0.553	Numeric (log Papp in 10-6 cm/s)
Absorption	Intestinal absorption (human)	93.49	Numeric (% Absorbed)
Absorption	Skin Permeability	-2.658	Numeric (log Kp)
Absorption	P-glycoprotein substrate	No	Categorical (Yes/No)
Absorption	P-glycoprotein I inhibitor	No	Categorical (Yes/No)
Absorption	P-glycoprotein II inhibitor	No	Categorical (Yes/No)
Distribution	VDss (human)	-0.372	Numeric (log L/kg)
Distribution	Fraction unbound (human)	0.436	Numeric (Fu)
Distribution	BBB permeability	-0.458	Numeric (log BB)
Distribution	CNS permeability	-2.868	Numeric (log PS)
Metabolism	CYP2D6 substrate	No	Categorical (Yes/No)
Metabolism	CYP3A4 substrate	No	Categorical (Yes/No)
Metabolism	CYP1A2 inhibitor	Yes	Categorical (Yes/No)
Metabolism	CYP2C19 inhibitor	No	Categorical (Yes/No)
Metabolism	CYP2C9 inhibitor	No	Categorical (Yes/No)
Metabolism	CYP2D6 inhibitor	No	Categorical (Yes/No)
Metabolism	CYP3A4 inhibitor	No	Categorical (Yes/No)
Excretion	Total Clearance	0.1	Numeric (log ml/min/kg)
Excretion	Renal OCT2 substrate	No	Categorical (Yes/No)
Toxicity	AMES toxicity	Yes	Categorical (Yes/No)
Toxicity	Max. tolerated dose (human)	0.843	Numeric (log mg/kg/day)
Toxicity	hERG I inhibitor	No	Categorical (Yes/No)
Toxicity	hERG II inhibitor	No	Categorical (Yes/No)
Toxicity	Oral Rat Acute Toxicity (LD50)	2.442	Numeric (mol/kg)
Toxicity	Oral Rat Chronic Toxicity (LOAEL)	1.366	Numeric (log mg/kg bw/day)
Toxicity	Hepatotoxicity	No	Categorical (Yes/No)
Toxicity	Skin Sensitisation	Yes	Categorical (Yes/No)
Toxicity	Pyriformis toxicity	1.298	Numeric (log ug/L)
Toxicity	Minnow toxicity	1.473	Numeric (log mM)

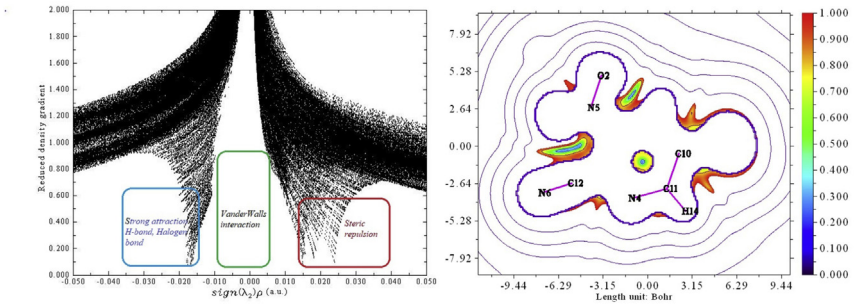

Figure 9. (a)Scatter graph of reduced density gradient RDG (NCI) and (b) color filled RDG of 5B3N2C molecule.

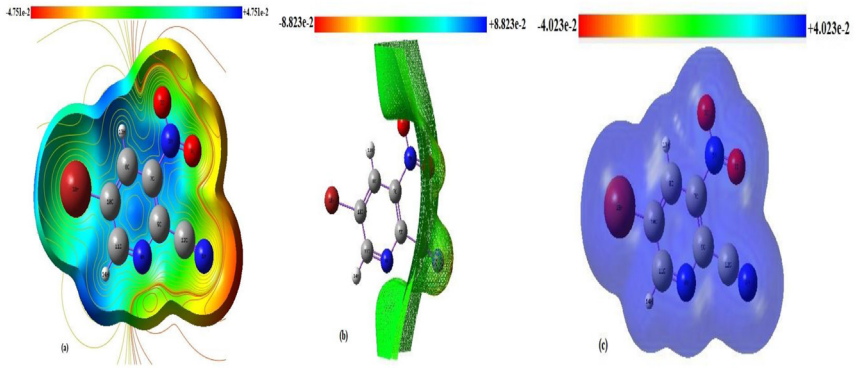

Figure 10. (a) Molecular electrostatic potential, (b) Electrostatic potential and (c)Total electron density of 5B3N2C molecule in gas phase.

studied molecule has none. It reveals that the 5B3N2C compound is a promising drug candidate for cancer.

3.9. Molecular docking

Molecular docking not only addresses the active drug reaction site, but also its binding affinity and other biological effects [50, 51]. The computational molecular docking was implemented to establish the binding conformations, binding energies, binding affinity, inhibition constants [52], of the 5B3N2C ligand with target protein. Centromere-associated protein E is a motor protein of the kinesin microtubule that plays an important role in incorporating the dynamics of microtubule chromosome interactions with the signalling of mitotic control points and has emerged as a novel cancer therapy target. The selected proteins of centromere associated protein inhibitor (CENP-E) was acquired from RCSB protein data bank, the PDB IDs are 3CEJ, 4CTH, 6DNB, 6SND. For context, Figures 11 and 12 displays the binding interaction conformations of the most of the proteins and ligands and the obtained docking constraints are exhibited in Table 9. Generally, by pi-alkyl, pi-pi, pi-donor hydrogen bond and conventional hydrogen bond interactions in molecular docking simulations, the ligand binds to docking sites of various proteins. The binding energy of the ligand with target protein, 3CEJ were found to be -6.19 kcal/mol and their inhibition constant value 28.78μM. The ligand was interacted with the donor amino acid residues ARG′309, ARG′309, ARG′310, ARG′310, ARG′242 at the distance 1.8–2.6 Å through five conventional hydrogen bond involving nucleophilic oxygen O3, O2 atom of nitro group and nitrogen N6 atom of nitrile group. The two pi-alkyl interactions form among the centre of the pyridine ring and acceptor residue PHE′196, and donor residue ARG′81.

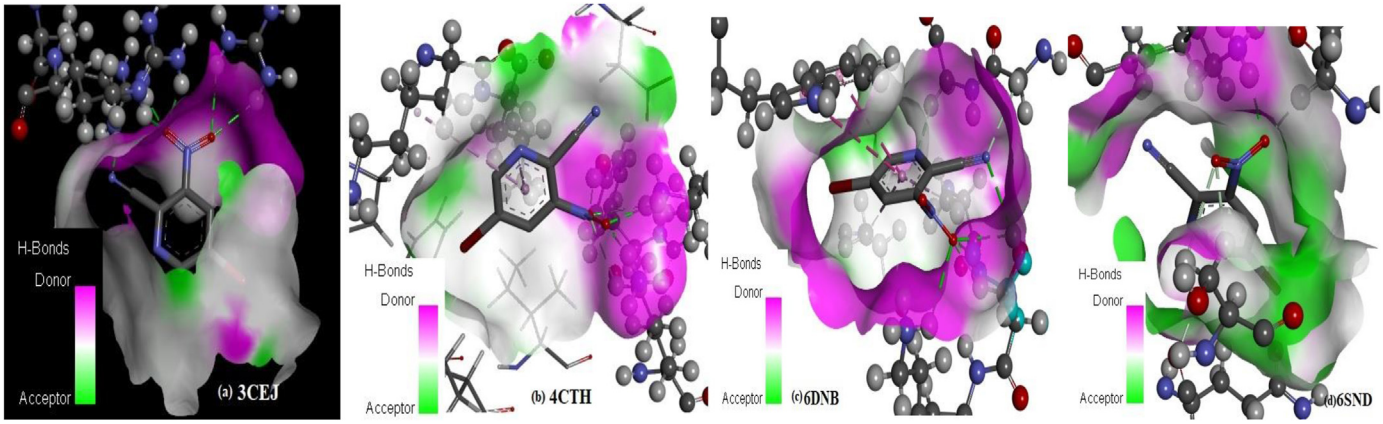

Figure 11. Binding mode of 5B3N2C with different proteins (a)3CEJ, (b)4CTH, (c)6DNB, (d)6SND.

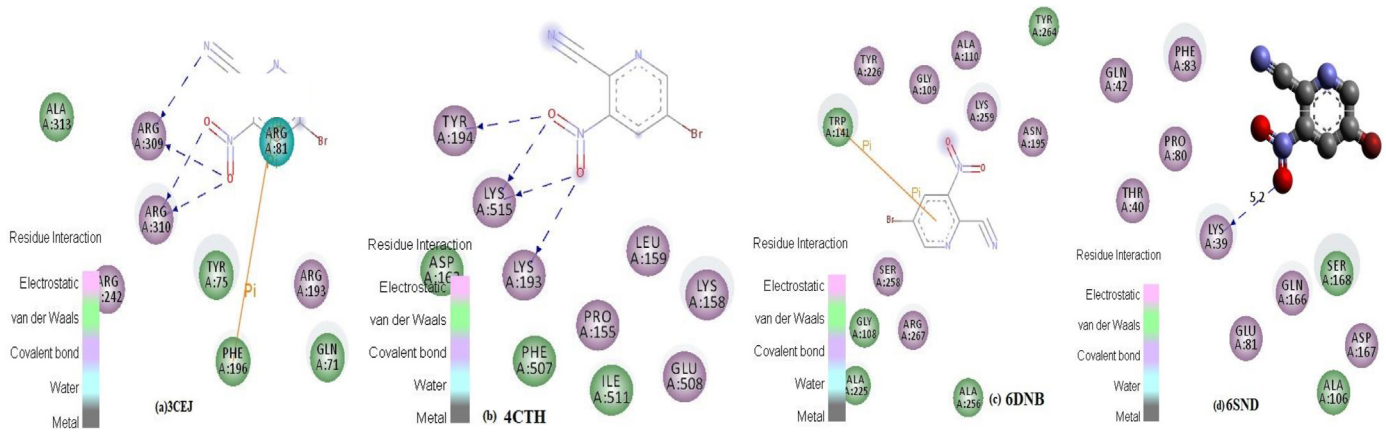

Figure 12. Binding mode of 5B3N2C with different proteins (a)3CEJ, (b)4CTH, (c)6DNB, (d)6SND in 2D mode.

Table 9. Binding affinity, Hydrogen bond interactions, Estimated inhibition constant of the 5B3N2C molecule with centromere associated inhibition proteins.

Protein (PDB ID)	No. of hydrogen bond interactions	Bond type	Bonded residues	Bonded distance(Å)	Hydrogen bond interactions	Estimated inhibition constant (μM)	Binding energy (kcal/mol)	Intermolecular energy (kcal/mol)	Reference RMSD(Å)
3CEJ	5	Conventional	ARG′309	2	N-2HH1	28.78	-6.19	-6.49	108.021
		and π-alkyl	ARG′309	1.8	O–-2HH2				
			ARG310	1.9	O–2HH2				
			ARG′242	2.6	O-2HH2				
			ARG′310	1.9	O-HE				
4CTH	4	Conventional	LYS′515	1.7	O-HZ1	28.44	-6.2	-6.5	29.531
			LYS′193	2.5	O-HZ1				
			LYS′193	2.6	O-HZ2				
			LYS′194	1.7	O-HH				
6DNB	2	Conventional	SER′258	2.8	N-HG	61.11	-5.75	-6.05	44.353
		and π-alkyl, π-stacked	SER′258	1.8	O-HG				
6SND	1	Conventional and carbon	LYS′39	2	O-HZ1	287.62	-4.83	-5.13	44.144

The binding energy of the ligand with target protein, 4CTH were established to be -6.20 kcal/mol and their inhibition constant value 28.44 μM. The ligand was interacted with the donor amino acid residues LYS′515, LYS′193, LYS′193, TYR′194 at the distance 1.7–2.6 Å through four conventional hydrogen bond involving nucleophilic oxygen O3, O2 atoms of nitro group. The ligand with the target protein, 6DNB were established to be -5.75 kcal/mol and their inhibition constant value 61.11 μM. The ligand was interacted with the donor amino residues SER′258, and SER′258 at the distance 1.8 and 2.8 Å through two conventional hydrogen bond involving oxygen O3, O2 atom of nitro group. The two pi-alkyl and pi-stacked interactions form among the ring and the donor residue TRP′141. The ligand with target protein, 6SND were established to be -4.83 kcal/mol and their inhibition constant 287.62 μM. The ligand was interacted with the amino residues LYS′39 at the distance 2.0Å. Of all the proteins 3CEJ and 4CTH was exhibited enhanced binding energy (-6.19 kcal/mol, and -6.20 kcal/mol) as compared with other proteins. Figures 11 and 12 shows the binding mode schematic, which confirms the development of interactions. It is therefore concluded that the designated compound may have the inhibitory property of centromere associated protein (CENP-E). Biological tests, on the other hand, are needed to confirm the computational assumptions.

3.10. Molecular dynamics

In molecular dynamics, force fields can be decomposed into bonded interactions comprised of Hooke's law potentials and non-bonded interactions comprised of Columbic and Vander Wall's interactions. The structure of the protein 3CEJ was derived from the protein data bank. SwissParam external methods were used to construct the 5B3N2C ligand topology. The structural features of the 3CEJ-5B3N2C complex were investigated using molecular dynamics simulations. The modified Berendsen thermostat and Parrinello-Rahman barostat settings were used to equilibrate the system's NVT and NPT. With a phase size of 0.002ps, equilibration was achieved. Figure 13 implies that the stabilization of the 3CEJ-5B3N2C, RMSD indicates the stability of complex

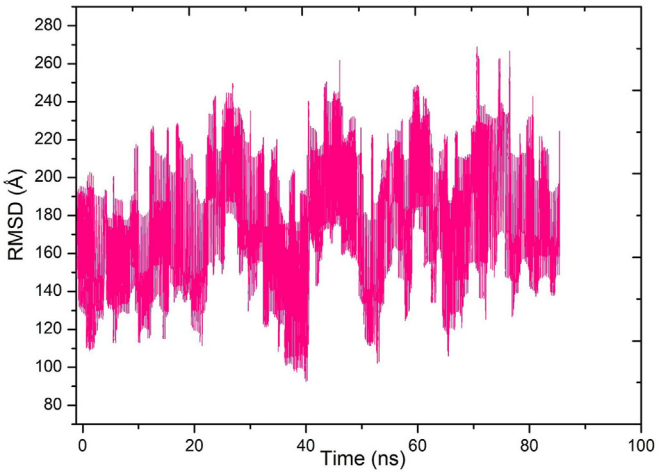

Figure 13. The RMSD stabilization in time of the back bone of the 3CEJ-5B3N2C complex.

forming. It is well accepted that hydrogen bonds that satisfy certain requirements aid protein–ligand interaction and structural stability.

3.11. Thermodynamic properties

The static thermodynamic functions for the free ligand were inferred from the theoretical harmonic frequencies relied on vibrational observation,: heat capability (Cp), enthalpy changes (H), entropy(S). The thermodynamic properties of heat capability (Cp), entropy (S) and enthalpy (H) for 5B3N2C are also dictated by temperature dependence. Up to the decomposition point of the studied compound, the thermodynamic properties such as heat capacity, entropy, and enthalpy were computed. The melting point is 101–109 °C, so that the 5B3N2C is unstable at 1000K. the thermodynamic properties are therefore measured at 500K. The Perl THERMO.PL [53] script has been used and is tabulated in Table 10. It is identified that, with temperatures varying from 100 to 500K, these thermodynamic functions are increasing due to the fact molecular vibrational intensities increase with the temperature. The association with temperature changes between heat capability, entropy, and enthalpy is a built-in quadratic formula. For these thermodynamic properties, the fitting factors (R^2) are respectively. The appropriate fitting Eqs. (II, III, IV) are as follows, and Figure 14 demonstrates the accepted statistical graphs [54].

$$S = 231.377 + 0.6866T–2.9577 \times 10^{-4}T^2 \ (R^2 = 0.99985) \quad \text{(II)}$$

$$Cp = 21.121 + 0.5112T–2.8141 \times 10^{-4}T^2 \ (R^2 = 0.99998) \quad \text{(III)}$$

$$H = -1.3243 + 0.0428T + 1.7189 \times 10^{-4}T^2 \ (R^2 = 0.99999) \quad \text{(IV)}$$

In the gas phase, all the thermodynamic measurements were performed and they could not be included in the solution. For more assessment on 5B3N2C, all these thermodynamic data provide helpful details. They can be used to quantify other thermodynamic functions, and according to the second thermodynamic law, to evaluate the path of chemical reactions.

Table 10. Thermodynamic properties of 5B3N2C molecule obtained by DFT/6-311++G(d,p).

T (K)	S (J/mol.K)	Cp (J/mol.K)	ddH (kJ/mol)
100	296.573	69.567	4.789
200	358.016	111.822	13.896
298.15	409.68	148.558	26.716
300	410.601	149.2	26.992
400	457.999	180.805	43.543
500	501.191	206.273	62.947

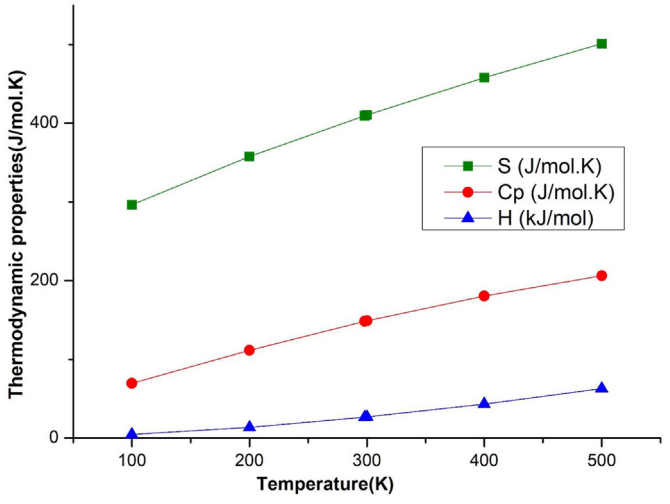

Figure 14. Correlation graphs of thermodynamic properties at different temperature for 5B3N2C molecule.

4. Conclusion

The geometrical parameters optimized were theoretically intended. The electronic properties were considered theoretically at 289nm and 309nm with maximum absorption wavelength. Using NBO analysis, the intermolecular interaction of the title compound was recognised and its MEP displays the potential targets of electrophilic and nucleophilic occurrences that are reactive. The measured electrophilic index was found to be 8.552. The polarizability calculations of title compound contribute to an efficient NLO material. The values of HOMO-LUMO energy gap (4.3903eV) affect the chemical stability and bioactivity of the molecule. For the group contribution of orbitals of molecule, DOS and PDOS were plotted. The molecular docking study against 3CEJ reveals substantial centromere protein inhibitor property that exhibits the lowest binding free energies at -6.19 kcal/mol. The thermodynamic properties are achieved in the 100K to 500 K scale. With increase in temperature, the gradients heat capability, entropy, and enthalpy increase.

Declarations

Author contribution statement

K. Arulaabaranam: Conceived and designed the experiments; Performed the experiments; Wrote the paper.

S. Muthu: Performed the experiments.

G. Mani: Analyzed and interpreted the data.

A. S. Ben Geoffrey: Contributed reagents, materials, analysis tools or data.

Funding statement

This research did not receive any specific grant from funding agencies in the public, commercial, or not-for-profit sectors.

Data availability statement

Data included in article/supplementary material/referenced in article.

Declaration of interests statement

The authors declare no conflict of interest.

Additional information

No additional information is available for this paper.

References

[1] Anatoly N. Vereshchagin, Michail N. Elinson, Yuliya E. Anisina, Fedor V. Ryzhkov, Alexander S. Goloveshkin, Mikhail P. Egorov, Synthesis, structural, spectroscopic and docking studies of new 5C-substituted 2,4-diamino-5H-chromeno[2,3-b] pyridine-3-carbonitriles, J. Mol. Struct. 1146 (15) (2017) 766–772.

[2] L. Ravindranath, B. Venkatram Reddy, Theoretical and experimental study of torsional potentials, molecular structure (monomer and dimer), vibrational analysis and molecular characteristics of some dimethyl bipyridines, J. Mol. Struct. 1200 (2020) 127089.

[3] S. Sivaprakash, S. Prakash, S. Mohan, Sujin P. Jose, Quantum chemical studies and spectroscopic investigations on 22-amino-3-methyl-5-nitropyridine by density functional theory, Heliyon 5 (2019), e02149.

[4] Pradeep R. Varadwaj, Arpita Varadwaj, Bih-Yaw Jin, Hexahalogenated and their mixed benzene derivatives as prototypes for the understanding of halogen···halogen intramolecular interactions: New insights from combined DFT, QTAIM-, and RDG-based NCI analyses, J. Comp. Chem. 36 (2015) 2328–2343.

[5] Jamelah S. Al-Otaibi, Tautomerization, molecular structure, transition state structure, and vibrational spectra of 2-aminopyridines: a combined computational and experimental study, SpringerPlus 4 (2015) 586.

[6] D. Shoba, S. Periandi, S. Boomadevi, S. Ramalingam, E. Fereyduni, FT-IR, FT-Raman, UV, NMR spectra, molecular structure, ESP, NBO and HOMO–LUMO investigation of 2-methylpyridine 1-oxide: A combined experimental and DFT study, Spectrochim. Acta, Part A 118 (2014) 438–447.

[7] J. Lorenc, Dimeric structure and hydrogen bonds in 2-N-ethylamino-5-metyl-4-nitro-pyridine studied by XRD, IR and Raman methods and DFT calculations, Vib. Spectrosc. 61 (2012) 112–123.

[8] A. Nataraj, V. Balachandran, T. Karthick, M. Karabacak, FT-Raman, FT-IR, UV spectra and DFT and ab initio calculations on monomeric and dimeric structures of 3, 5-pyridinedicarboxylic acid, Atac J. Mol. Struct. 1027 (2012) 1–14.

[9] Jayachandran Jayakumar, Tien-Lin Wu, Min-Jie Huang, Pei-Yun Huang, Tsu-Yu Chou, Hao-Wu Lin, Chien-Hong Cheng, Pyridine-carbonitrile–carbazole-based delayed fluorescence materials with highly congested structures and excellent OLED performance, ACS Appl. Mater. Interfaces 11 (2019) 21042–21048.

[10] Wei Liu, Cai-Jun Zheng, Kai Wang, Zhan Chen, Dong-Yang Chen, Li Fan, Xue-Mei Ou, Yuping Dong, Xiao-Hong Zhang, Novel carbazol-pyridine-carbonitrile derivative as excellent blue thermally activated delayed fluorescence emitter for highly efficient organic light-emitting devices. ACS applied materials & interfaces, ACS Appl. Mater. Interfaces 7 (34) (2015) 18930–18936.

[11] Raju Ranjith Kumar, Subbu Perumal, Palaniappan Senthilkumar, Perumal Yogeeswari, Dharmarajan Sriram, An atom efficient, solvent-free, green synthesis and antimycobacterial evaluation of 2-amino-6-methyl-4-aryl-8-[(E)-arylmethylidene]-5,6,7,8-tetrahydro-4H-pyrano[3,2-c]pyridine-3-carbonitriles. Bioorg. Med. Chem. Lett 17 (2007) 6459–6462.

[12] Adel S. Girgis, Nawal Mishriky, Mohey Ellithey, Hanaa M. Hosnia, Hanaa Farag, Novel synthesis of [1]-benzothiepino[5,4-b]pyridine-3-carbonitriles and their anti-inflammatory properties, Bioorg. Med. Chem. 15 (2007) 2403–2413.

[13] Diane H. Boschelli, Biqi Wu, Ana Carolina Barrios Sosa, Joan Chen, Magda Asselin, Derek C. Cole, Julie Lee, Xiaoke Yang, Divya Chaudhary, Synthesis and PKCtheta inhibitory activity of a series of 4-(indol-5-ylamino)thieno[2,3-b]pyridine-5-carbonitriles. Bioorg. Med. Chem. Lett 18 (2008) 2850–2853.

[14] Diane H. Boschelli, Biqi Wu, Ana Carolina Barrios Sosa, Haris Durutlic, Joan J. Chen, Yan Wang, Jennifer M. Golas, Judy Lucas, Frank Boschelli, Synthesis and Src kinase inhibitory activity of 2-phenyl- and 2-thienyl-7-phenylaminothieno[3,2-b]pyridine-6-carbonitriles. J. Med. Chem. 48 (2005) 3891–3902.

[15] Adnan A. Bekhit, Azza M. Baraka, Novel milrinone analogs of pyridine-3-carbonitrile derivatives as promising cardiotonic agents. Eur. J. Med. Chem. 40 (2005) 1405–1413.

[16] Wiebke Fugel, Anselm Erich Oberholzer, Bernhard Gschloessl, Dzikowski Ron, Narkiss Pressburger, Preu Lutz, Laurence H. Pearl, Blandine Baratte, Morgane Ratin, Ilya Okun, Christian Doerig, Sebastian Kruggel, Thomas Lemcke, Laurent Meijer, Conrad Kunick, 3,6-Diamino-4-(2-halophenyl)-2-benzoylthieno[2,3-*b*]pyridine-5-carbonitriles Are Selective Inhibitors of *Plasmodium falciparum* Glycogen Synthase Kinase-3, J. Med. Chem. 1 (56) (2013) 264–275.

[17] Dominik Naglav, Briac Tobey, Benjamin Lyhs, Beate Römer, Dieter Bläser, Christoph Wölper, Georg Jansen, Stephan Schulz, Synthesis, solid-state structure, and bonding analysis of a homoleptic beryllium azide, Angew. Chem. Int. Ed. 56 (29) (2017) 8559–8563.

[18] Rizk E. Khidre, Ameen A. Abu-Hashem, Mohamed El-Shazly, Synthesis and anti-microbial activity of some 1-substituted amino-4, 6-dimethyl-2-oxo-pyridine-3-carbonitrile derivatives, Eur. J. Med. Chem. 46 (2011) 5057–5064.

[19] Adel S. Girgis, Nasser S.M. Ismail, Hanaa Farag, Facile synthesis, vasorelaxant properties and molecular modeling studies of 2-amino-8a-methoxy-4H-pyrano [3, 2-c] pyridine-3-carbonitriles, European J. Med. Chem. 46 (2011) 2397–2407.

[20] V. Krishnakumar, S. Muthunatesan, FT-IR, FT-Raman spectra and scaled quantum mechanical study of 2,3-dihydroxy pyridine and 2,4-dihyroxy-3-nitropyridine, Spectrochim. Acta, Part A 65 (2006) 818–825.

[21] A.D. Becke, Density-functional thermochemistry. III. The role of exact exchange, J. Chem. Phys. 98 (1993) 5648–5652.

[22] A.D. Becke, Density-functional exchange-energy approximation with correct asymptotic behavior, Phys. Rev. 38 (1988) 3098–3100.

[23] C. Lee, W. Yang, R.G. Parr, Development of the Colle-Salvetti correlation-energy formula into a functional of the electron density, Phys. Rev. B 37 (1988) 785–789.

[24] C.N.R. Rao, Ultraviolet and Visible Spectroscopy, Chemical Applications, Plenum Press, New York, 1975.

[25] N.M. O'Boyle, A.L. Tenderholt, K.M. Langner, cclib: a library for package-independent computational chemistry algorithms, J. Compd. Chem. 29 (2008) 839–845.

[26] A. Frisch, Hrant P. Hratchian, R.D. Dennington II, T.A. Keith, J. Milliam, A.B. Nielsen, A.J. Holder, J. Hiscocks, GaussView Reference, Version 5.0, Gaussian, Semichem. Inc., Wallingford CT, USA, 2009.

[27] T. Lu, F. Chen, Multiwfn: A multifunctional wavefunction analyzer, J. Comput. Chem. 33 (2012) 580–592.

[28] H.M. Berman, The Protein Data Bank, Nucleic Acids Res. 28 (2000) 235–242.

[29] G.M. Morris, R. Huey, W. Lindstrom, M.F. Sanner, R.K. Belew, D.S. Goodsell, A.J. Olson, AutoDock4 and AutoDockTools4: Automated docking with selective receptor flexibility, J. Comp. Chem. 30 (2009) 2785–2791.

[30] Dassault Systemes BIOVIA, [Discovery Studio 4.1 Visualizer], Dassault Systemes, San Diego, 2014.

[31] D.V.D. Spoel, E. Lindahl, B. Hess, G. Greonhof, A.E. Mark, H.J.C. Berendsen, GROMACS: High performance molecular simulations through multi-level parallelism from laptops to supercomputers, J. Comput. Chem. 26 (2005) 1701–1718.

[32] R.A. Nagalakshmi, J. Suresh, S. Maharani, R. Ranjith Kumar, P.L. Nilantha Lakshman, Crystal structures of 2-benzylamino-4-(4-bromophenyl)-6,7,8,9-tetrahydro-5H-cyclohepta[b]- pyridine-3-carbonitrile and 2-benzylamino-4-(4-chlorophenyl)-6,7,8,9-tetrahydro-5H-cyclohepta- [b]pyridine-3-carbonitrile, Acta Crystallogr. E71 (2015) 12–15.

[33] D.A. Kleinman, Nonlinear dielectric polarization in optical media, Phys. Rev. 126 (1962) 1977–1979.

[34] S. Premkumar, A. Jawahar, T. Mathavan, M. KumaraDhas, A. MiltonFranklin Benial, Vibrational spectroscopic and DFT calculation studies of 2-amino-7-bromo-5-oxo-[1]benzopyrano [2,3-b]pyridine-3 carbonitrile, Spectrochim. Acta, Part A 138 (5) (2015) 252–263.

[35] S. Muthu, E. Isac Paulraj, Spectroscopic and molecular structure (monomeric and dimeric structure) investigation of 2-[(2-hydroxyphenyl) carbonyloxy] benzoic acid by DFT method: A combined experimental and theoretical study, J. Mol. Struct. 1038 (2013) 145–162.

[36] Horiye Yahyaei, Mehrnoosh Khaleghian, Synthesis, geometry optimization, spectroscopic investigations (UV/Vis, excited states, FT-IR) and application of new azomethine dyes, J. Mol. Struct. 1148 (15) (2017) 134–149.

[37] Shakeel Ahmad Khan, Komal Rizwan, Sammia Shahid, Mahmoud A. Noamaan, Tahir Rasheed, Amjad Hira, Synthesis, DFT, computational exploration of chemical reactivity, molecular docking studies of novel formazan metal complexes and their biological applications, Appl. Organomet. Chem. 34 (3) (2020) e5444.

[38] LiYuan Bin Shi, Yuan Yuan TianyuTang, Yanlin Tang, Study on electronic structure and excitation characteristics of cyclo[18]carbon, Chem. Phys. Lett. 741 (2020) 16, 136975.

[39] H. Jacobsen, Localized-orbital locator (LOL) profiles of chemical bonding, Can. J. Chem. 86 (2008) 695–702.

[40] Christer B. Aakeroy, Mark Nieuwenhuyzen, Sarah L. Price, Three polymorphs of 2-Amino-5-nitropyrimidine: experimental structures and theoretical predictions, J. Am. Chem. Soc. 120 (35) (1998) 8986–8993.

[41] V. Tsirelson, A. Stash, Determination of the electron localization function from electron density, Chem. Phys. Lett. 351 (1–2) (2002) 142–148.

[42] R.A. Boto, J.P. Piquemal, Contreras-Garcia, Revealing strong interactions with the reduced density gradient: a benchmark for covalent, ionic and charge-shift bonds, J. Theor Chem Acc (2017) 136–139.

[43] Nyiang Kennet Nkungli, Julius Numbonui Ghogomu, Theoretical analysis of the binding of iron (III) protoporphyrin IX to 4-methoxyacetophenone thiosemicarbazone via DFT-D3, MEP, QTAIM, NCI, ELF, and LOL studies, J. Mol. Model. 23 (7) (2017) 1–20.

[44] J.S. Murray, K. Sen, Molecular Electrostatic Potentials: Concepts and Applications, Elsevier, Amsterdam, 1996.

[45] P. Politzer, J.S. Murray, D.L. Beveridge, R. Lavery (Eds.), Protein, 2, Adenine Press, Schenectady, NY, 1991 (Chapter 13).

[46] Manju Pandey, S. Muthu, N.M. Nanje Gowda, Quantum mechanical and spectroscopic (FT-IR, FT-Raman, ^{1}H, ^{13}C NMR, UV-Vis) studies, NBO, NLO, HOMO, LUMO and Fukui function analysis of 5-Methoxy-1H-benzo[d]imidazole-2(3H)-thione by DFT studies, J. Mol. Struct. 1130 (15) (2017) 511–521.

[47] Leena Khanna, Sugandha Singhal, Subhash C. Jain, Pankaj Khanna, Spiro-indole-coumarin hybrids: synthesis, ADME, DFT, NBO studies and in silico screening through molecular docking on DNA G-Quadruplex, Chem. Select 5 (2020) 3420–3433.

[48] C.A. Lipinski, Rule of five in 2015 and beyond: Target and ligand structural limitations, ligand chemistry structure and drug discovery project decisions, Adv. Drug Deliv. Rev. 101 (2016) 34–41.

[49] www.molinspiration.com/services/properties.html.

[50] S. Christopher Jeyaseelan, A. Milton Franklin Benial, Spectroscopic characterization, DFT studies, molecular docking and cytotoxic evaluation of 4-nitro-indole-3-carboxaldehyde: A potent lung cancer agent, J. Mol. Recogn. (2020), e2872.

[51] Naveen Ram Kumar Tittal, Ghule D. Vikas, Poonam Rani, Kashmiri Lal, Ashwani Kumar, Synthesis, antimicrobial activity, molecular docking and DFT study: Aryl-Carbamic Acid 1-Benzyl-1 H -[1,2,3]Triazol-4-ylmethyl Esters, Chem. Select 5 (2020) 6723–6729.

[52] J.C. Prasana, S. Muthu, C.S. Abraham, Molecular docking studies, charge transfer excitation and wave function analyses (ESP, ELF, LOL) on valacyclovir : A potential antiviral drug, Comput. Biol. Chem. 78 (2019) 9–17.

[53] K.K. Irikura, P.L. Thermo, Natl. Instit. Stan. Technol. Gaithersburg, MD, (2002).

[54] K. Arulaabaranam, S. Muthu, G. Mani, S. Sevvanthi, Quantum mechanical computation, spectroscopic exploration and molecular docking analysis of 2-Bromo-4-fluoroacetanilide, J. Mol. Struct. (2020) 1220, 128639.